

Video Article

Development of a 3D Graphene Electrode Dielectrophoretic Device

Hongyu Xie¹, Radheshyam Tewari², Hiroyuki Fukushima³, Jeffri Narendra³, Caryn Heldt¹, Julia King¹, Adrienne R. Minerick¹¹Department of Chemical Engineering, Michigan Technological University²Department of Mechanical Engineering, Michigan Technological University³XG Sciences, Inc.Correspondence to: Adrienne R. Minerick at minerick@mtu.eduURL: <https://www.jove.com/video/51696>DOI: [doi:10.3791/51696](https://doi.org/10.3791/51696)

Keywords: Physics, Issue 88, graphene paper, dielectrophoresis, graphene electrodes, 3D laminated microdevice, polystyrene beads, cell diagnostics

Date Published: 6/22/2014

Citation: Xie, H., Tewari, R., Fukushima, H., Narendra, J., Heldt, C., King, J., Minerick, A.R. Development of a 3D Graphene Electrode Dielectrophoretic Device. *J. Vis. Exp.* (88), e51696, doi:10.3791/51696 (2014).

Abstract

The design and fabrication of a novel 3D electrode microdevice using 50 μm thick graphene paper and 100 μm double sided tape is described. The protocol details the procedures to construct a versatile, reusable, multiple layer, laminated dielectrophoresis chamber. Specifically, six layers of 50 μm x 0.7 cm x 2 cm graphene paper and five layers of double sided tape were alternately stacked together, then clamped to a glass slide. Then a 700 μm diameter micro-well was drilled through the laminated structure using a computer-controlled micro drilling machine. Insulating properties of the tape layer between adjacent graphene layers were assured by resistance tests. Silver conductive epoxy connected alternate layers of graphene paper and formed stable connections between the graphene paper and external copper wire electrodes. The finished device was then clamped and sealed to a glass slide. The electric field gradient was modeled within the multi-layer device. Dielectrophoretic behaviors of 6 μm polystyrene beads were demonstrated in the 1 mm deep micro-well, with medium conductivities ranging from 0.0001 S/m to 1.3 S/m, and applied signal frequencies from 100 Hz to 10 MHz. Negative dielectrophoretic responses were observed in three dimensions over most of the conductivity-frequency space and cross-over frequency values are consistent with previously reported literature values. The device did not prevent AC electroosmosis and electrothermal flows, which occurred in the low and high frequency regions, respectively. The graphene paper utilized in this device is versatile and could subsequently function as a biosensor after dielectrophoretic characterizations are complete.

Video Link

The video component of this article can be found at <https://www.jove.com/video/51696/>

Introduction

Graphene is a novel material known for its high quality electronic properties and potential chemical and biosensor applications¹. Graphene nanoplatelets have been used for catalyst support^{2,3}, biosensors⁴, super-capacitors⁵, and composite-electrodes including graphene/polyaniline and silicon nanoparticle/graphene composites⁶⁻⁸. This manuscript describes utilization of graphene paper as electrodes in a unique three-dimensional (3D), layered microfluidic device. Graphene paper electrodes were laminated with insulative double-sided tape and a chamber drilled within which 3D AC dielectrophoresis of polystyrene beads was performed.

Dielectrophoresis (DEP) refers to the movement of polarizable particles under non-uniform electrical fields. Positive DEP (pDEP) or negative DEP (nDEP) occurs when particles are more or less polarizable than the surrounding medium, resulting in movement toward the strongest or weakest electrical field, respectively. This nonlinear electrokinetic tool has been used for separation, sorting, trapping, and identification of particles and biological cells⁹⁻¹⁵. The dielectrophoretic force experienced by a polarized particle is a function of the electric field gradient, particle radius and shape, particle dielectric properties including conductivity and permittivity, as well as the media conductivity and permittivity. In traditional two-dimensional (2D) DEP, particle movement is in the primary plane of the electric field gradient typically formed between microfabricated surface electrodes; movement in the vertical direction is negligible compared to in-plane directions in most devices. However, harnessing this third dimension of electrical field gradients for 3D DEP allows for higher sample throughput and increases the versatility to design new and improved dielectrophoretic separations in which the flow is traverse to the field gradients^{16,17}. Other specific designs include 3D insulator-based DEP¹⁸, 3D carbon-electrode DEP^{13,19}, and 3D electroplating DEP¹⁰. As evidenced by the research into 3D structures, such devices can be operated in continuous flow mode to achieve higher throughputs. Observation of the 3D particle movement in our layered 3D device is achieved as a function of frequency and medium conductivity via light microscopy at different focal heights.

Fatoyinbo *et al.* first reported DEP in a 3D laminated electrode/insulation structure using alternatively stacked 30 μm aluminum foil and 150 μm epoxy resin films²⁰. Hubner *et al.* then designed similar 3D laminated electrodes with 35 μm copper tape and 118 μm polyimide adhesive²¹. This work borrows the 3D-well design^{22,23}, and uniquely utilizes the convenience of 50 μm graphene paper as the conducting layers and 100 μm double-sided tape as the insulating layers, which achieved sealing and sufficient electrical shielding. Graphene paper versatility is a distinct advantage for 3D electrode microdevices because the graphene nanoplatelets have the ability to concurrently act as biosensors, which this group previously demonstrated²⁴.

The field gradients achieved within the graphene paper/polymer laminated 3D microdevices depend on the micro-well dimensions, the graphene paper layers, and the applied electric field. Critical dimensions include the vertical electrode spacing (conducting and insulating layer thicknesses) and micro-well diameter and height (determined by layers stacked). The electric signal can be tuned via amplitude and frequency. The current device structure is for batch operation, but can be tailored to a continuous flow device. The device fabrication technique described here is suitable for developing 3D laminated electrodes with a wide variety of graphene nanoplatelet properties simply by exchanging the graphene paper utilized. Advantages of utilizing graphene paper are versatility of physical and chemical properties, reduced expense, and the graphene nanoplatelets can concurrently act as biosensors to detect a wide range of bioanalytes²⁴. Long-term goals of high throughput 3D DEP systems are to rapidly identify cell types²⁵⁻²⁷, or achieve label-free, electrically mediated cell sorting of diseased cells from populations of healthy cells²⁸. This paper demonstrates material optimization and device preparation and operation followed by illustration and analysis of typical results.

Protocol

1. Fabricate a Laminated Electrode/insulation 3D Structure

- For a 6 graphene layer, 5 tape layer device, cut graphene paper with a scalpel or similar razor blade and straight-edged ruler into six 0.7 cm x 1.5 cm rectangles and use scissors to cut double-sided pressure-sensitive tape into five 1.3 cm x ~5 cm stripes.
NOTE: As shown in **Figure 1a**, this yields a 3 ground electrode, 3 AC signal electrode device. The 7 mm conducting layer width is narrow enough to fit onto a glass slide, yet wide enough for easy drilling. The 2 mm length does not easily break upon repeated use and has sufficient room to attach copper wires. The device depth is limited by end mill depths.
- Lay the first layer of graphene paper on a clean glass slide. Slowly cover one end of the graphene paper with one stripe of tape, leaving a ~2 mm margin to assure insulation between the two adjacent graphene paper layers (**Figure 1b**).
- Place the second layer of graphene paper on the top of the tape offset to the first layer of graphene paper (**Figure 1a**). Apply moderate pressure (press uniformly with thumb, ~100 N over 0.7 cm² area) after addition of each conducting layer to ensure good sealing between layers.
- Repeat steps 1.2 and 1.3 for the remaining layers, leaving both the top and bottom layers graphene paper. Cut along the dotted line shown in **Figure 1b** to remove the excess tape from the device edges leaving a small ~1 mm margin to assure sealed insulation between graphene paper layers (**Figure 1b**).
NOTE: Double-sided tape is not utilized as the top and bottom layers to avoid collecting debris as this laminated structure is drilled, mounted on a slide, and filled with sample.
- Perform a quick insulation test with a multimeter (resistance mode). Position the positive and negative probes on two different sides of the device (A and B on **Figure 1c**); high resistance (kilo- to mega-Ohms) indicates good insulation between layers. Remove the layered structure from the glass slide to prepare for micro-well drilling.
NOTE: A device typically fails the insulation test when adjacent graphene paper layers make contact during steps 1.2 through 1.4. Discard such devices.

2. Drill Micro-well in the Laminated Structure

- Use a computer-controlled mechanical micro-milling machine and choose an end mill with a 700 μm in diameter and 2.1 mm length of cut. Immobilize the laminated structure on the micro-milling stage using appropriate clamps (**Figures 2a** and **b**). Run the milling machine spindle at 8,600 rpm, then lower the end mill slowly into and through the center of the laminated structure. Move the rotating end mill up and down through the micro-well to smooth the inside wall.
 - Choose micro-well diameters, which are constrained by available end mill diameter/length of cut aspect ratios. Ensure that the inner surface of micro-well is as vertical and clean as possible for optimal electric field gradients and light passage through the micro-well.
- Clean debris from micro-well with pressurized air. Perform another insulation test as described in 1.5.

3. Attach Electrical Leads to the Laminated Structure

- Fold two 3 cm long 32 G copper wires to a right angle at 2 cm. Mix ~1.5 ml of part A and B of silver conductive epoxy.
NOTE: $\rho_{\text{copper}} = 1.68 \times 10^{-8} \Omega \cdot \text{m}$, $\rho_{\text{silver epoxy}} = 1.7 \times 10^{-4} \Omega \cdot \text{m}$
- Manually apply mixed silver epoxy to the top and the tips of all 3 graphene paper layers to assure good contact between layers on side A of the laminated structure (**Figure 1c**), then place the 1 cm copper wire end in the epoxy and between any two layers. Softly squeeze the layers to remove excess epoxy and assure good electrical contact. Repeat for side B of the laminated structure.
- Place the whole device in oven rack, to dry overnight 70 °C at and 1 atm.

4. Prepare Sample and Media

- Prepare isotonic media of a spectrum of conductivities using the conductivity meter, 290 mM mannitol stock solution and serial additions of isotonic phosphate buffer saline (PBS).
NOTE: A linear correlation exists between the conductivity and volume concentration of ~290 mOsm/L PBS (conducting) in ~290 mOsm/L mannitol solution (non-conducting). The video features a medium of 0.01 S/m conductivity.
- Mix polystyrene beads with prepared conductivity media or e-pure water (~5 x 10⁻⁶ S/m) to a 1:50 vol:vol ratio. This protocol is easily adaptable to biological cells as well.

5. Setup Experiment and Operate Device

1. Clamp the device onto a glass slide with moderate pressure (**Figure 2d**) using modified paper clamps or equivalent. The footings should be close enough to the micro-well to seal the laminated structure to the glass slide preventing sample leakage. The clamp should fit within the microscope stage with pressure optimized to a) prevent deformation of the laminated structure, and b) ensure the micro-well fluid does not leak. Deformation alters the well geometry and light path reducing experiment reproducibility.
2. Using a micro syringe or equivalent, slowly inject $\sim 1 \mu\text{l}$ of the sample into the micro-well and avoid introducing any bubbles. Repeat injection if necessary and use care to not damage the micro-well walls with the sharp needle. Slightly overfill the micro-well and immediately slide cover glass over the micro-well to remove excess fluid, prevent evaporation, and ensure reproducible volumes for each experiment.
NOTE: A diamond tip glasscutter works well to score and crack cover glass to size.
3. Secure the completed laminated microdevice to the microscope stage and attach the function generator electrode wires to the two copper leads on the device. In AxioVision (Zeiss software), click button to start the camera recording in multidimensional acquisition mode. Initiate function generator signal at a fixed time period after starting the CCD camera recording to document responses with and without the electric field applied.
NOTE: Here 100 Hz to 10 MHz frequency with a $15 V_{\text{peak-peak}}$ signal were applied and experiments were observed at 10X magnification at 1 to 200 above the glass slide surface for 2 sec without field and ~ 5 min with field applied. Images were digitally saved at 1 to 5 frames per sec (fps) for further analysis.
4. Upon experiment completion, remove the device and dismantle the clamps. Immerse both the glass slide and device in soapy water, then rinse well. Reuse devices about 30 times with consistent performance.

6. Data Analysis and Image Processing

1. Analyze image data with preferred software, such as ImageJ. Calculate velocity from the particle displacement between consecutive images at a given time step.
2. Calculate experimental DEP force and field strength based on velocity to compile trends and compare with theory²⁹.
3. Measure particle velocity radially in the micro-well geometry consistent with the shape of the electric field gradient. From the micro-well edge to the center, identify 8 concentric isoelectric contours (350, 300, ..., 50, 0 μm), which results in 7 regions.
NOTE: The time for particles to traverse the 50 μm distance was used to calculate velocity. When geometric variations necessitated it, the isoelectric contours were adjusted slightly.

Representative Results

Dielectrophoretic experiments on 6 μm polystyrene beads were conducted in a 0.38 mm^3 cylindrical micro-well. Results demonstrate that a 3D laminated graphene paper-based device can illustrate similar dielectrophoretic signatures as 3D metal foil laminated devices^{20,21}, traditional 2D metal-electrode^{26,27}, and 2D insulator devices²⁵. In the following experiments, an $15 V_{\text{peak-peak}}$ AC signal was applied and frequency was varied from 100 Hz to 10 MHz³⁰. Qualitative DEP results are shown in **Figure 3** at time 0 before field application (first column) and after 5 min (second column) in the electric field. When no electrical field was present, particles slowly sediment to the device bottom via gravity (**Figures 3a** and **b**). **Figure 3c** and **d** demonstrate typical pDEP results at 1 kHz, as indicated by particles gathering toward the micro-well edges. **Figure 3e** and **f** illustrate nDEP at 10 MHz, as indicated by focusing of particles in the center.

Figure 4a illustrates the experimental DEP responses for conductivities between 0.0001 S/m and 1.3 S/m over a frequency range from 100 Hz to 10 MHz. Negative DEP (nDEP) or positive DEP (pDEP) was typically determined by the observation of beads moving toward the center or the edges of the micro-well. However, this is complicated by recirculating flows (20-50 μm diameter) near the edges of the micro-well that happened simultaneously with DEP behavior at two regions in the conductivity-frequency space as shown by open symbols in **Figure 4a**. One type of recirculating flow was observed below ~ 10 kHz at all conductivities tested while the other type was observed at high conductivity and high frequency. The recirculating flows alter nDEP or pDEP bead motions to varying degrees. These concurrent forces are illustrated in the parameter space in **Figure 4a**.

Dielectrophoretic velocities are tabulated as a function of radial position using concentric counters (**Figure 5a**) within the micro-well. Velocity trends with position are shown in **Figure 5c**. As expected, the highest velocities are observed near the micro-well edge, which corresponds to the region with the highest electric field density (**Figure 5b**). Particles move vertically in and out of the focal plane during a 1 min recording. However, this vertical velocity magnitude is estimated to be and therefore is negligible compared to the 5-100 $\mu\text{m}/\text{sec}$ concentric velocity measured. In-plane velocities range from 5 $\mu\text{m}/\text{sec}$ to 36 $\mu\text{m}/\text{sec}$, which correspond to DEP mobilities of $\approx 1.07 \times 10^{-16} \text{ m}^4/(\text{V}\#\text{sec})$ over the electric field density regions of $5 \times 10^4 \text{ V/m}$ to $3 \times 10^5 \text{ V/m}$. Velocities are consistent with those reported in 3D systems^{31,32}, 2D electrode systems³³, and DC insulator DEP systems³⁴.

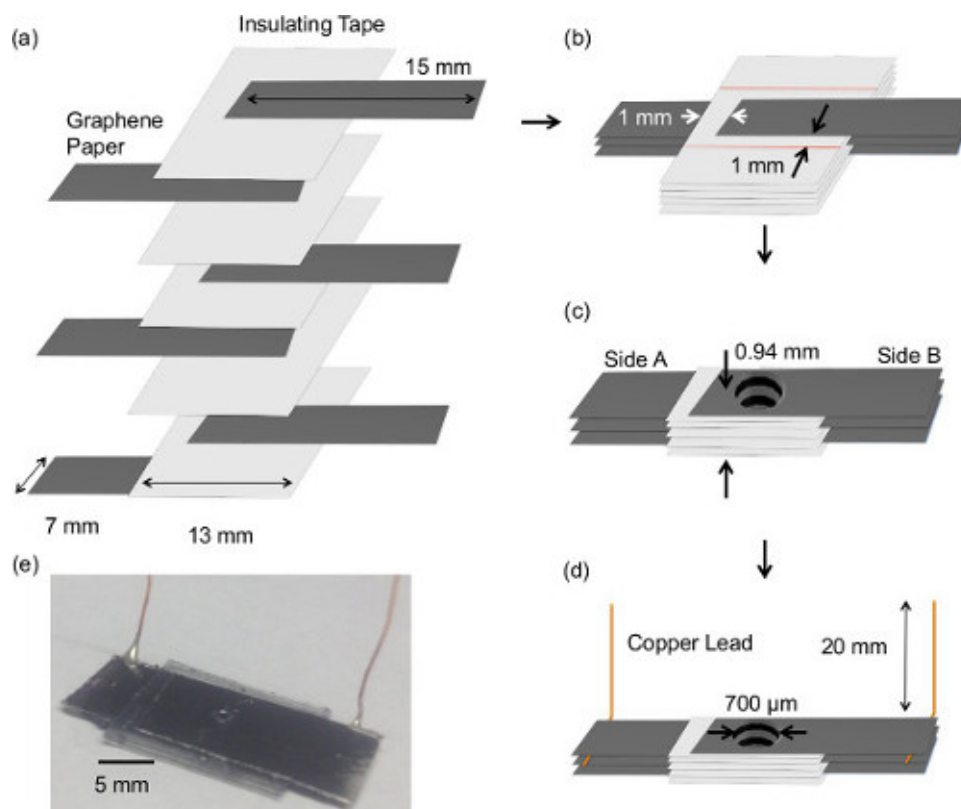


Figure 1. Fabrication process for the laminated device. a) Alternately stack 6 layers of graphene paper and 5 layers of double sided tape to prevent connection between adjacent graphene layers. b) Press layers together and cut excess double-sided tape along the red dashed line. c) Drill a micro-well in the center via micro-milling as shown in **Figures 2a** and **b**. d) Adhere two copper leads to Side A and Side B with silver epoxy. e) Final fabricated device.

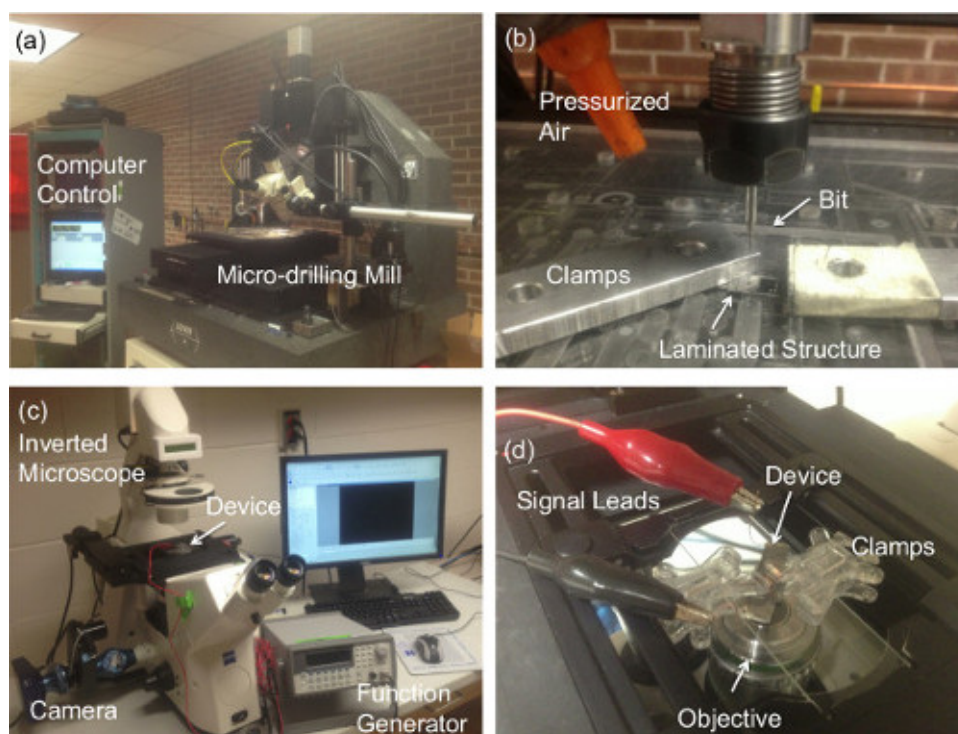


Figure 2. a) Computer-controlled micro-drilling machine. b) Laminated structure is immobilized on the stage with clamps. Pressurized air is used to blow debris off the end mill. c) Microdevice experiments are conducted with a microscope, CCD camera, function generator and computer for data acquisition. d) Close-up view of microdevice clamped onto a glass slide on the microscope stage. AC electrical signal from the function generator is applied to the device through the copper leads.

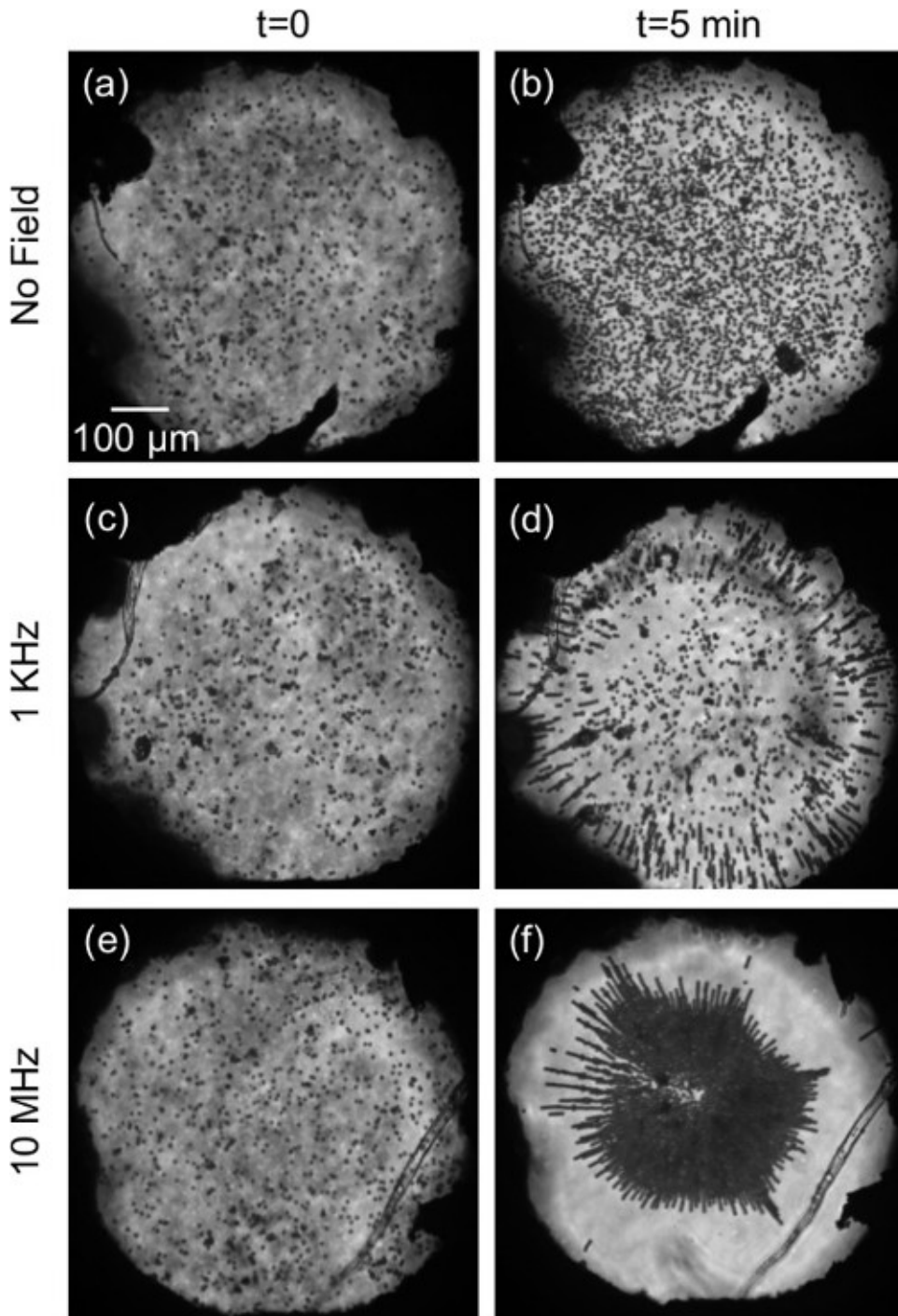


Figure 3. Typical dielectrophoresis responses within the 3D laminated microdevice. A $15 V_{\text{peak-peak}}$ was applied with a medium conductivity of $1.3 \times 10^{-4} \text{ S/m}$. The first column illustrates particles at experiment start with the electric field off, and the second column shows the response after 5 min. **a-b)** Particles sediment to the micro-well bottom; **c-d)** at 1 kHz, particles gathered near the micro-well edge, indicating pDEP. **e-f)** At 10 MHz, particles focused to the micro-well center, indicating nDEP.

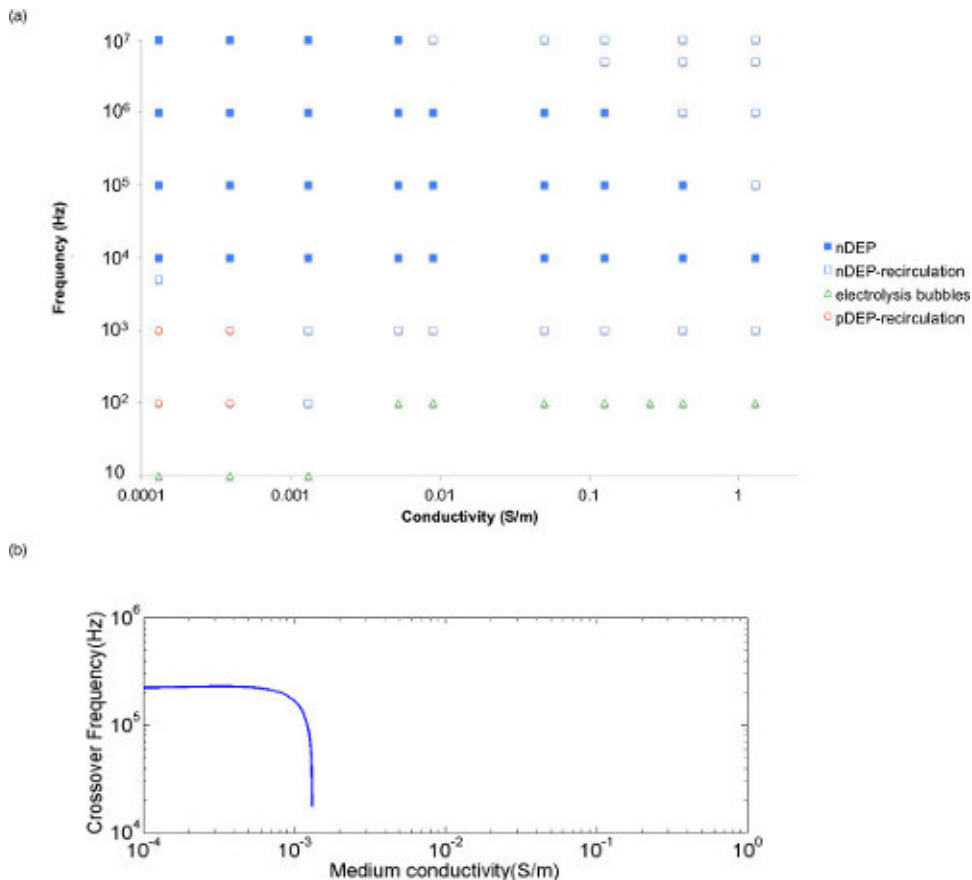


Figure 4. a) Experimental DEP behavior of 6.08 μm polystyrene beads as a function of conductivity (0.0001-1.3 S/m) and frequency (100 Hz-10 MHz) in PBS adjusted mannitol solution. Small recirculations were observed concurrent with DEP behavior near micro-well edges for low frequencies (<1 kHz) and all tested medium conductivities, as well as at high frequencies and higher medium conductivity. Open symbols \square and \circ represent negative DEP and positive DEP with recirculation, while the solid symbol \blacksquare represents nDEP without recirculation. Below \sim 100 Hz, electrolysis bubbles were observed and are represented by Δ . b) Predicted crossover frequencies from 0.0001 S/m to 1.3 S/m. [Please click here to view a larger version of this figure.](#)

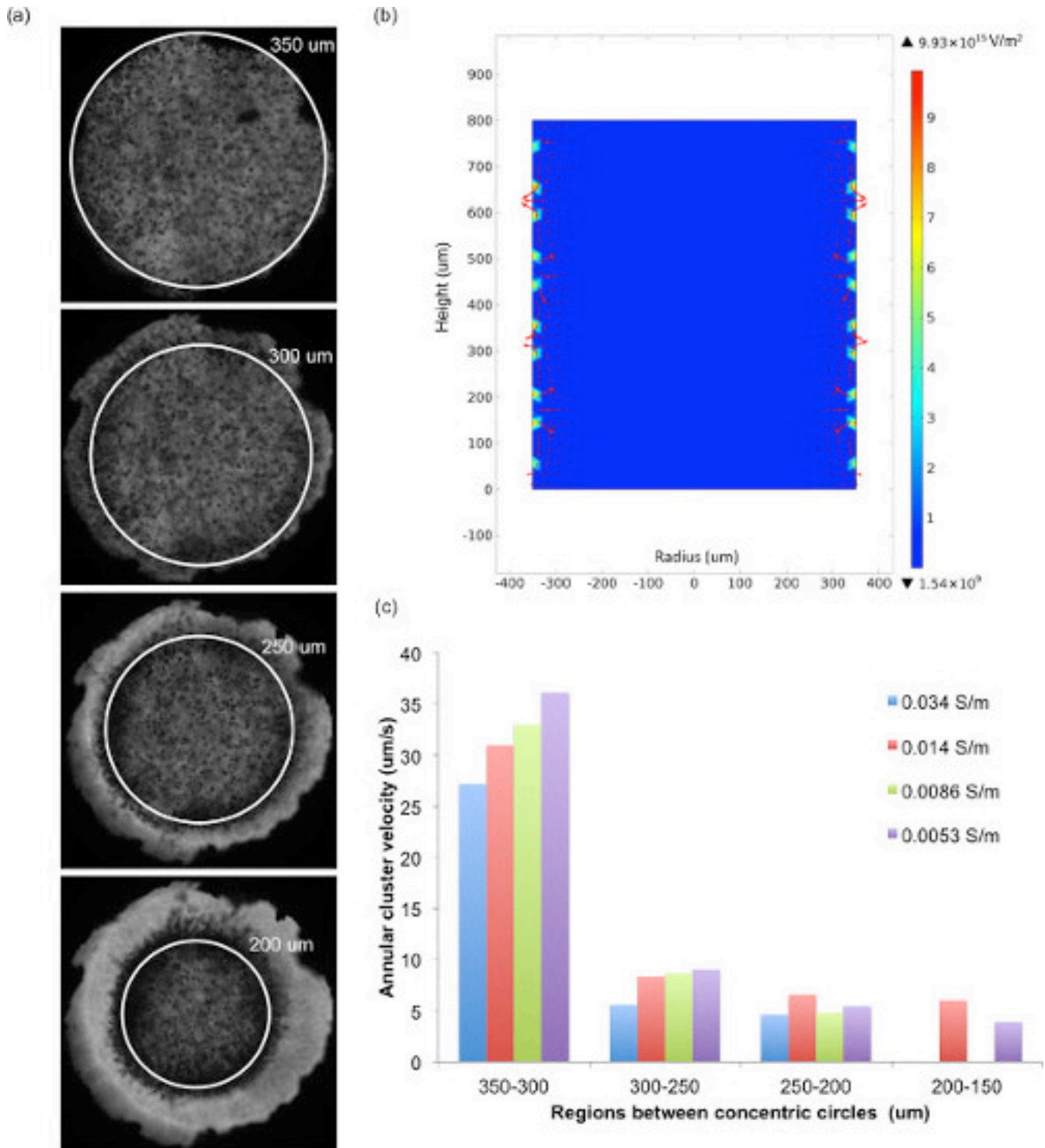


Figure 5. a) Images of polystyrene beads experiencing nDEP in a 15 $V_{\text{peak-peak}}$, 1MHz field. Concentric circles track the movement of particles as they traverse the microwell. b) COMSOL simulation of electric field gradient (V/m^2) of a cross-section of micro-well. c) Dielectrophoretic velocities of clusters of beads as a function of radial position within the micro-well. [Please click here to view a larger version of this figure.](#)

Discussion

This manuscript details protocols for fabricating a novel 6 graphene layer and 5 tape layer microdevice. Further, device operation is illustrated via observed DEP behaviors of 6.08 μm polystyrene beads along with a unique, geometrically relevant particle velocity analysis approach. This versatile approach to construct nonlinear electrokinetic devices is less costly than electrode and fluidic layer microfabrication techniques, while yielding equally reliable results.

Further, this novel 3D graphene paper microdevice yielded experimental dielectrophoretic results that agree with both the theoretically predicted behavior and previously reported experimental results³⁵. For signal frequencies from 100 Hz up to 10 MHz and media conductivities from 1×10^{-4} S/m to 1.3 S/m, experiments verified the existence of a crossover frequency, below which pDEP was observed and above which nDEP was observed. As expected, nDEP was observed over most of the conductivity-frequency space as shown in **Figure 4a**. Theory predicts that $6.08 \mu\text{m}$ homogeneous polystyrene beads ($\epsilon_p = 2.55$, $\sigma_p = 1.3 \times 10^{-3}$ S/m³⁶) have a crossover frequency when $\sigma_m < \sigma_p = 1.3 \times 10^{-3}$ S/m. In the remaining parameter space from 1×10^{-4} S/m to approximately 1.3×10^{-3} S/m, crossover frequencies (f_{co} on the order of ≈ 1 kHz) were observed. For example, f_{co} was 1 kHz in a 3.9×10^{-4} S/m medium, while a previous reported experimental result at 1.0×10^{-3} S/m was $f_{co} = 5$ kHz³⁵, and model-based predicted value was 168 kHz³⁷⁻³⁹. These three results are considered in rough agreement given the sensitivity of crossover frequency to change in medium conductivity in the specific region⁴⁰, as well as other compounding charge induced factors and equipment variations. As shown in **Figure 4b**, as media conductivity changes slightly from 1×10^{-4} S/m to 1.3×10^{-3} S/m, corresponding crossover frequencies decrease 2 orders of magnitude or more. Using 168 kHz as the crossover frequency in the model, with parameters fixed as specified above, one can solve for the particle conductivity and find it to be 1.00×10^{-3} S/m compared to the real value of 1.3×10^{-3} S/m (23% difference).

Observations of two types of recirculating flows in the conductivity-frequency space were observed and attributed to AC electroosmosis and electrothermal flows in the low and high frequency regions, respectively. For low frequencies (<10 kHz) at all tested medium conductivities, local particle recirculation velocities increased as frequency decreased with slight changes due to medium conductivity. Both the conductivity-frequency conditions and size of the recirculating rolls (20-50 μm) agree with previous AC electroosmotic flow studies⁴¹⁻⁴³. For relative high frequencies (>100 kHz) at relative high medium conductivity (>0.01 S/m), nDEP begins to be overpowered by recirculation. Recirculating particle velocities increased as the medium conductivity increased and frequency increased. Again, both the conductivity-frequency conditions and the size of recirculations agree with previous findings⁴⁴⁻⁴⁷.

In 3D DEP, particles also experience dielectrophoretic forces pushing particles between adjacent graphene paper layers at multiple vertical positions in the micro-well. The optical microscope observation of this is partially compromised because light is scattered by focused DEP particles above and below the plane of interest. Due to gravity sedimentation over time, more particles were observed near the bottom DEP focusing planes than in the upper-most DEP focusing planes (data not shown)⁴⁸.

Device fabrication is extremely versatile; the protocols provided can be easily adapted for devices with more layers or other materials. As an alternative insulation layer material, polydimethylsiloxane (PDMS) thin films can be spincoated to a controllable and fairly uniform thickness. PDMS has well characterized electrical and surface chemistry properties, but handling such thin fragile films was troublesome. Double-sided tape has more uniform thickness, was easier to handle with better layer-to-layer sealing and thus yielded higher success rate of optimally functional devices. The XG Sciences graphene paper (Leaf B-072) functioned well as an electrode material and tailored manufacturing offered versatile electrical and mechanical qualities. Higher nanoplatelet concentrations reduced paper resistivity²⁴ and polymeric supports prevented water adsorption while cellulosic supports allow water diffusion (data not shown).

Complications with device functionality can include increased resistivity at the well surface, broken electrical connections, electrolytic bubbles, bubble introduction during sample loading, and skewed well geometry. The insulation test in procedure step 1.5 should be utilized prior to each experiment to assess device integrity. The utilized XG graphene paper surface exposed to the microwell wore off after ~ 30 experiments. Inconsistent DEP results were easily recognized via erratic global flow through the micro-well or no response to an applied potential. Side A and Side B (**Figure 1c**) graphene layers of the device may break if not handled gently. In these cases, replacement devices are needed. At frequencies at or below 100 Hz, the 3D graphene electrodes catalyzed water electrolysis to produce O_2 and H_2 bubbles. This frequency threshold is 2 orders of magnitude lower than this group's previous results with traditional microfabricated 2D electrodes⁴⁹, which expands the operating space in which particles or biological cells can be interrogated. Air bubbles from the sample syringe should be avoided due to electric field shape and optical interferences. Lastly, perfectly vertical micro-well drilling is critical for consistent optical illumination and observation of DEP behaviors. Micro-well skewing becomes more difficult to manage as the number of laminated layers increases. Most confocal and light microscopes have working distances below 1 mm, so DEP behaviors cannot be easily observed at thickness above this. However, increasing the third dimension would be advantageous for large scale DEP processing.

A straightforward laminated graphene paper/tape structure has been demonstrated as a batch-wise 3D DEP microdevice. In future applications, particle or cell suspension could continuously flow through the device to achieve higher-throughput DEP sorting⁵⁰. Specific biomedical applications that require sorting of large volumes to separate and identify rare cells include detection of circulating tumor cells⁵¹ and sepsis⁵². In addition, water-absorbing graphene paper could simultaneously function as an electrode and diffusion medium for particle/cell concentrators. Lastly, graphene paper has been demonstrated as a viable biosensor²⁴. The device described here could be used for simultaneous DEP concentration and biological detection at the graphene surface. Thus, different graphene paper types may be useful electrodes in high throughput microfluidic systems employing electrokinetics and/or biosensors.

Disclosures

The authors have no conflicts to disclose.

Acknowledgements

Thanks to XG Sciences for generous donations of graphene paper. Thanks to Dr. C. Friedrich for generously letting us use the micro-drilling equipment. A special thanks is extended to Tayloria Adams for narrating the video.

References

1. Geim, A.K. and Novoselov, K.S. The rise of graphene. *Nature Materials*. **6** (3), 183-191, Doi 10.1038/Nmat1849 (2007).

2. Jafri, R.I., Rajalakshmi, N., and Ramaprabhu, S. Nitrogen doped graphene nanoplatelets as catalyst support for oxygen reduction reaction in proton exchange membrane fuel cell. *Journal of Materials Chemistry*. **20** (34), 7114-7117, Doi 10.1039/C0jm00467g (2010).
3. Kavan, L., Yum, J.H., and Gratzel, M. Graphene Nanoplatelets Outperforming Platinum as the Electrocatalyst in Co-Bipyridine-Mediated Dye-Sensitized Solar Cells. *Nano Letters*. **11** (12), 5501-5506, Doi 10.1021/Nl203329c (2011).
4. Aravind, S.S.J., Baby, A.T.T., Arockiadoss, T., Rakhi, R.B., and Ramaprabhu, S. A cholesterol biosensor based on gold nanoparticles decorated functionalized graphene nanoplatelets. *Thin Solid Films*. **519** (16), 5667-5672, Doi 10.1016/J.Tsf.2011.03.032 (2011).
5. Si, P., Ding, S.J., Lou, X.W., and Kim, D.H. An electrochemically formed three-dimensional structure of polypyrrole/graphene nanoplatelets for high-performance supercapacitors. *Rsc Advances*. **1** (7), 1271-1278, Doi 10.1039/C1ra00519g (2011).
6. Wang, D.-W. *et al.* Fabrication of Graphene/Polyaniline Composite Paper via *In Situ* Anodic Electropolymerization for High-Performance Flexible Electrode. *ACS Nano*. **3** (7), 1745-1752, 10.1021/nn900297m (2009).
7. Lee, J.K., Smith, K.B., Hayner, C.M., and Kung, H.H. Silicon nanoparticles-graphene paper composites for Li ion battery anodes. *Chem Commun (Camb)*. **46** (12), 2025-7, 10.1039/b919738a (2010).
8. Kavan, L., Yum, J.H., and Gratzel, M. Optically Transparent Cathode for Dye-Sensitized Solar Cells Based on Graphene Nanoplatelets. *Acc Nano*. **5** (1), 165-172, Doi 10.1021/Nn102353h (2011).
9. Martinez-Duarte, R., Microfabrication technologies in dielectrophoresis applications--a review. *Electrophoresis*. **33** (21), 3110-32, 10.1002/elps.201200242 (2012).
10. Yamamoto, M. *et al.* Patterning with particles using three-dimensional interdigitated array electrodes with negative dielectrophoresis and its application to simple immunosensing. *Electrochimica Acta*. **82**, 35-42, Doi 10.1016/J.Electacta.2012.02.109 (2012).
11. Doh, I., Kim, Y., and Cho, Y.H. A particle trapping chip using the wide and uniform slit formed by a deformable membrane with air bubble plugs. *Current Applied Physics*. **13** (5), 902-906, Doi 10.1016/J.Cap.2013.01.025 (2013).
12. Lin, S.C., Lu, J.C., Sung, Y.L., Lin, C.T., and Tung, Y.C. A low sample volume particle separation device with electrokinetic pumping based on circular travelling-wave electroosmosis. *Lab on a Chip*. **13** (15), 3082-3089, Doi 10.1039/C3lc50343g (2013).
13. Martinez-Duarte, R., Camacho-Alanis, F., Renaud, P., and Ros, A. Dielectrophoresis of lambda-DNA using 3D carbon electrodes. *Electrophoresis*. **34** (7), 1113-22, 10.1002/elps.201200447 (2013).
14. Yang, S.M., Tseng, S.Y., Chen, H.P., Hsu, L., and Liu, C.H. Cell patterning via diffraction-induced optoelectronic dielectrophoresis force on an organic photoconductive chip. *Lab on a Chip*. **13** (19), 3893-3902, Doi 10.1039/C3lc50351h (2013).
15. Srivastava, S.K., Gencoglu, A., and Minerick, A.R. DC insulator dielectrophoretic applications in microdevice technology: a review. *Anal Bioanal Chem*. **399** (1), 301-21, 10.1007/s00216-010-4222-6 (2011).
16. Liao, S.H., Cheng, I.F., and Chang, H.C. Precisely sized separation of multiple particles based on the dielectrophoresis gradient in the z-direction. *Microfluidics and Nanofluidics*. **12** (1-4), 201-211, Doi 10.1007/S10404-011-0863-9 (2012).
17. Bajaj, P., Marchwiany, D., Duarte, C., and Bashir, R. Patterned three-dimensional encapsulation of embryonic stem cells using dielectrophoresis and stereolithography. *Adv Healthc Mater*. **2** (3), 450-8, 10.1002/adhm.201200318 (2013).
18. Braff, W.A., Pignier, A., and Buie, C.R. High sensitivity three-dimensional insulator-based dielectrophoresis. *Lab Chip*. **12** (7), 1327-31, 10.1039/c2lc21212a (2012).
19. Martinez-Duarte, R., Gorkin, R.A., 3rd, Abi-Samra, K., and Madou, M.J. The integration of 3D carbon-electrode dielectrophoresis on a CD-like centrifugal microfluidic platform. *Lab Chip*. **10** (8), 1030-43, 10.1039/b925456k (2010).
20. Fatoyinbo, H.O., Kamchis, D., Whittingham, R., Ogin, S.L., and Hughes, M.P. A high-throughput 3-D composite dielectrophoretic separator. *Ieee Transactions on Biomedical Engineering*. **52** (7), 1347-1349, Doi 10.1109/Tbme.2005.847553 (2005).
21. Hubner, Y., Hoettges, K.F., Kass, G.E.N., Ogin, S.L., and Hughes, M.P. Parallel measurements of drug actions on Erythrocytes by dielectrophoresis, using a three-dimensional electrode design. *Ieee Proceedings-Nanobiotechnology*. **152** (4), 150-154, DOI 10.1049/ip-nbt:20050011 (2005).
22. Abdul Razak, M.A., Hoettges, K.F., Fatoyinbo, H.O., Labeed, F.H., and Hughes, M.P. Efficient dielectrophoretic cell enrichment using a dielectrophoresis-well based system. *Biomicrofluidics*. **7** (6), 64110, 10.1063/1.4842395 (2013).
23. Hughes, M.P., O.S., Hoettges, K.F., Wattingham, R. *Device for Dielectrophoretic Manipulation of Particles.*, (2005).
24. Heldt, C.L. *et al.* Stacked graphene nanoplatelet paper sensor for protein detection. *Sensors and Actuators B-Chemica*. **181**, 92-98, Doi 10.1016/J.Snb.2013.01.041 (2013).
25. Srivastava, S.K., Artemiou, A., and Minerick, A.R. Direct current insulator-based dielectrophoretic characterization of erythrocytes: ABO-Rh human blood typing. *Electrophoresis*. **32** (18), 2530-2540, Doi 10.1002/Elps.201100089 (2011).
26. Leonard, K.M. and Minerick, A.R. Explorations of ABO-Rh antigen expressions on erythrocyte dielectrophoresis: Changes in cross-over frequency. *Electrophoresis*. **32** (18), 2512-2522, Doi 10.1002/Elps.201100077 (2011).
27. Srivastava, S.K., Daggolu, P.R., Burgess, S.C., and Minerick, A.R. Dielectrophoretic characterization of erythrocytes: Positive ABO blood types. *Electrophoresis*. **29** (24), 5033-5046, Doi 10.1002/Elps.200800166 (2008).
28. Minerick, A.R. The rapidly growing field of micro and nanotechnology to measure living cells. *AIChE Journal*. **54** (9), 2230-2237, 10.1002/aic.11615 (2008).
29. Garza-Garcia, L.D., Perez-Gonzalez, V.H., Perez-Sanchez, O.A., and Lapizco-Encinas, B.H. Electrokinetic Mobilities Characterization and Rapid Detection of Microorganisms in Glass Microchannels. *Chemical Engineering & Technology*. **34** (3), 371-378, Doi 10.1002/Ceac.201000298 (2011).
30. Lopez-de la Fuente, M.S. *et al.* An electric stimulation system for electrokinetic particle manipulation in microfluidic devices. *Rev Sci Instrum*. **84** (3), 035103, 10.1063/1.4793559 (2013).
31. Chen, D.F., Du, H., and Li, W.H. A 3D paired microelectrode array for accumulation and separation of microparticles. *Journal of Micromechanics and Microengineering*. **16** (7), 1162-1169, Doi 10.1088/0960-1317/16/7/008 (2006).
32. Chu, H., Doh, I., and Cho, Y.H. A three-dimensional (3D) particle focusing channel using the positive dielectrophoresis (pDEP) guided by a dielectric structure between two planar electrodes. *Lab on a Chip*. **9** (5), 686-691, Doi 10.1039/B812213j (2009).
33. Millet, L.J., Park, K., Watkins, N.N., Hsia, K.J., and Bashir, R. Separating beads and cells in multi-channel microfluidic devices using dielectrophoresis and laminar flow. *J Vis Exp*. (48), 10.3791/2545 (2011).
34. Weiss, N.G. *et al.* Dielectrophoretic mobility determination in DC insulator-based dielectrophoresis. *Electrophoresis*. **32** (17), 2292-7, 10.1002/elps.201100034 (2011).
35. Auerswald, J. and Knapp, H.F. Quantitative assessment of dielectrophoresis as a micro fluidic retention and separation technique for beads and human blood erythrocytes. *Microelectronic Engineering*. **67-8**, 879-886, Doi 10.1016/S0167-9317 (03)00150-3 (2003).

36. Park, S., Zhang, Y., Wang, T.H., and Yang, S. Continuous dielectrophoretic bacterial separation and concentration from physiological media of high conductivity. *Lab on a Chip*. **11** (17), 2893-2900, Doi 10.1039/C1lc20307j (2011).
37. Sun, T., Holmes, D., Gawad, S., Green, N.G., and Morgan, H. High speed multi-frequency impedance analysis of single particles in a microfluidic cytometer using maximum length sequences. *Lab on a Chip*. **7** (8), 1034-1040, 10.1039/B703546B (2007).
38. Hughes, M.P. and Morgan, H. Dielectrophoretic Characterization and Separation of Antibody-Coated Submicrometer Latex Spheres. *Analytical Chemistry*. **71** (16), 3441-3445, 10.1021/ac990172i (1999).
39. Liang, W.F. *et al.* Simultaneous separation and concentration of micro- and nano-particles by optically induced electrokinetics. *Sensors and Actuators a-Physical*. **193**, 103-111, Doi 10.1016/J.Sna.2013.01.020 (2013).
40. White, C.M., Holland, L.A., and Famouri, P. Application of capillary electrophoresis to predict crossover frequency of polystyrene particles in dielectrophoresis. *Electrophoresis*. **31** (15), 2664-2671, Doi 10.1002/Elps.201000086 (2010).
41. Wu, J., Ben, Y.X., Battigelli, D., and Chang, H.C. Long-range AC electroosmotic trapping and detection of bioparticles. *Industrial & Engineering Chemistry Research*. **44** (8), 2815-2822, Doi 10.1021/le049417u (2005).
42. Zhou, H., White, L.R., and Tilton, R.D. Lateral separation of colloids or cells by dielectrophoresis augmented by AC electroosmosis. *J Colloid Interface Sci*. **285** (1), 179-91, 10.1016/j.jcis.2004.11.040 (2005).
43. Green, N.G., Ramos, A., Gonzalez, A., Morgan, H., and Castellanos, A. Fluid flow induced by nonuniform ac electric fields in electrolytes on microelectrodes. I. Experimental measurements. *Phys Rev E Stat Phys Plasmas Fluids Relat Interdiscip Topics*. **61** (4 Pt B), 4011-8 (2000).
44. Green, N.G., Ramos, A., Gonzalez, A., Castellanos, A., and Morgan, H. Electrothermally induced fluid flow on microelectrodes. *Journal of Electrostatics*. **53** (2), 71-87, Doi 10.1016/S0304-3886 (01)00132-2 (2001).
45. Gonzalez, A., Ramos, A., Morgan, H., Green, N.G., and Castellanos, A. Electrothermal flows generated by alternating and rotating electric fields in microsystems. *Journal of Fluid Mechanics*. **564**, 415-433, Doi 10.1017/S0022112006001595 (2006).
46. Park, S., Koklu, M., and Beskok, A. Particle trapping in high-conductivity media with electrothermally enhanced negative dielectrophoresis. *Anal Chem*. **81** (6), 2303-10, 10.1021/ac802471g (2009).
47. Sin, M.L., Gau, V., Liao, J.C., and Wong, P.K. Electrothermal Fluid Manipulation of High-Conductivity Samples for Laboratory Automation Applications. *JALA Charlottesville Va*. **15** (6), 426-432, 10.1016/j.jala.2010.05.004 (2010).
48. Liao, S.-H., Cheng, I.F., and Chang, H.-C. Precisely sized separation of multiple particles based on the dielectrophoresis gradient in the z-direction. *Microfluidics and Nanofluidics*. **12** (1-4), 201-211, 10.1007/s10404-011-0863-9 (2012).
49. Gencoglu, A. and Minerick, A. Chemical and morphological changes on platinum microelectrode surfaces in AC and DC fields with biological buffer solutions. *Lab on a Chip*. **9** (13), 1866-1873, Doi 10.1039/B820126a (2009).
50. Bocchi, M. *et al.* Dielectrophoretic trapping in microwells for manipulation of single cells and small aggregates of particles. *Biosensors & Bioelectronics*. **24** (5), 1177-1183, Doi 10.1016/J.Bios.2008.07.014 (2009).
51. Li, P., Stratton, Z.S., Dao, M., Ritz, J., and Huang, T.J. Probing circulating tumor cells in microfluidics *Lab on a Chip*. (2013).
52. Rimmele, T. and Kellum, J.A. Clinical review: Blood purification for sepsis. *Critical Care*. **15** (1), Doi 10.1186/Cc9411 (2011).